deviation between the simulation and the measurement is attributed to parasitic reactive components between a coaxial balun and the antenna.

In addition, we measured the tag sensitivity ($P_{\mathrm{tag\ min.}}$) of fabricated tags on various materials in an anechoic chamber, using a commercial measurement system, Tagformance Lite of Voyantic Corporation [18]. We then calculated the maximum reading distance using (1) and (2). Fig. 8 presents the reading characteristic derived from the measured tag sensitivity when the tags are mounted on the decoupler, foam ($\mathrm{thickness} = 5$ mm), FR4 ($\mathrm{thickness} = 5$ mm), and glass ($\mathrm{thickness} = 4.8$ mm). As shown in Fig. 8, although the measured results have the operating frequency shift of 12 MHz from 912 MHz to 900 MHz, the suggested tag has only 5.1 m ($P_{\mathrm{tag\ min.}} = 5.3$ dB) deviation from 6.2 m ($P_{\mathrm{tag\ min.}} = -11.4$ dBm) to 11.3 m ($P_{\mathrm{tag\ min.}} = -16.7$ dBm) at 912 MHz. Such a small deviation in reading performance is similar to that of the tag in [19] where deviation in tag sensitivity is only 3.2 dB for various dielectric materials.

Hence, the proposed label tag is applicable to both dielectric and metallic objects by just adding the simple underlying radiator without modifying the label tag. In addition, the underlying radiator could be applied to commercial tags with the T-matching loop by simply modifying the structure, and used for curved metallic objects by employing flexible substrate.

IV. Conclusion

We proposed a novel RFID tag antenna and a decoupler in the UHF band which can be attached to various dielectric materials as well as metallic objects. Good impedance matching is achieved by geometrically adjusting vertical and horizontal length of the cross-shaped feeding loop. After a parameter study and optimization, the optimized antenna was manufactured and measured. The optimized tag has half-power bandwidth of 65 MHz (7.1%) and 17 MHz (1.9%), in free space and on the underlying radiator, respectively. We confirmed that the expected reading distance on both cases is over about 6.2 m under the condition of 36 dBm EIRP at 912 MHz. The suggested antenna would be suitable for practical RFID applications dealing with dielectric and metallic materials.

References

[1] K. Finkenzeller, *RFID Handbook: Radio-Frequency Identification Fundamentals and Applications*, 2nd ed. New York, NY, USA: Wiley, 2004.

[2] P. V. Nikitin, K. V. S. Rao, and S. Lazar, "An overview of near field UHF RFID," in *Proc. IEEE Int. Conf. on RFID*, Mar. 2007, pp. 167–174.

[3] K. V. S. Rao, P. V. Nikitin, and S. F. Lam, "Antenna design for UHF RFID tags: A review and a practical application," *IEEE Trans. Antennas Propag.*, vol. 53, pp. 3870–3876, Dec. 2005.

[4] R. F. Harrington, "On the gain and beamwidth of directional antenna," *IRE Trans. Antennas Propag.*, vol. 6, no. 3, pp. 219–225, Jul. 1958.

[5] J. S. Mclean, "A re-examination of the fundamental limits on the radiation Q of electrically small antenna," *IEEE Trans. Antennas Propag.*, vol. 44, no. 5, pp. 672–676, May 1996.

[6] C. A. Balanis, *Antenna Theory Analysis and Design*, 2nd ed. New York, NY, USA: John Wiley & Sons, 1997, pp. 86–88.

[7] J. Choo, J. Ryoo, J. Hong, C. Choi, and M. Tentzeris, "T-matching networks for the efficient matching of practical RFID tags," in *Proc. 39th Eur. Microw. Conf.*, Italy, 2009, pp. 5–8.

[8] T. Deleruyelle, P. Pannier, M. Egels, and E. Bergeret, "An RFID tag antenna tolerant to mounting on materials," *IEEE Antennas Propag. Mag.*, vol. 52, no. 4, pp. 14–19, Aug. 2010.

[9] Y. Okano, "A simple shape broadband planar antenna adaptable to RFID-tag," *IEEE Trans. Antennas Propag.*, vol. 54, no. 6, pp. 1885–1888, Jun. 2006.

[10] K.-H. Kim, J.-G. Song, D.-H. Kim, H.-S. Hu, and J.-H. Park, "Fork-shaped RFID tag antenna mountable on metallic surfaces," *Electron. Lett.*, vol. 43, no. 23, pp. 1400–1402, 2007.

[11] L. Mo, H. Zhang, and H. Zhou, "Broadband UHF RFID tag antenna with a pair of U slots mountable on metallic objects," *Electron. Lett.*, vol. 44, no. 20, pp. 1173–1774, 2008.

[12] P. H. Yang, Y. Li, L. Jiang, W. C. Chew, and T. T. Ye, "Compact metallic RFID tag antennas with a loop-fed method," *IEEE Trans. Antennas Propag.*, vol. 59, no. 12, pp. 4454–4462, Aug. 2011.

[13] K. H. Lin, S. L. Chen, and R. Mittra, "A looped-bowtie RFID tag antenna design for metallic objects," *IEEE Trans. Antennas Propag.*, vol. 61, no. 2, pp. 449–505, Feb. 2013.

[14] H. D. Chen, S. H. Kuo, C. Y. D. Sim, and C. H. Tsai, "Coupling-feed circularly polarized RFID tag antenna mountable on metallic surface," *IEEE Trans. Antennas Propag.*, vol. 60, no. 5, pp. 2166–2174, May 2012.

[15] J. Ryoo, J. Choo, and H. Choo, "Novel UHF RFID tag antenna for metallic foil package," *IEEE Trans. Antennas Propag.*, vol. 60, no. 1, pp. 377–379, Jan. 2012.

[16] Alien Higgs 3 Datasheet [Online]. Available: http://www.alientechnology.com/docs/products/DS_H3.pdf

[17] HFSS 13.2. [Online]. Available: http://www.ansys.com

[18] Tagformance Lite [Online]. Available: www.voyantic.com

[19] B. D. Braaten, M. Reich, and J. Glower, "A compact meander-line UHF RFID tag antenna loaded with elements found in right/left-handed coplanar waveguide structures," *IEEE Antennas Wireless Propag. Lett.*, vol. 8, pp. 1158–1161, 2009.

An Integrated Wide-Band Circularly Polarized Antenna for Millimeter-Wave Applications

Mohammad Fakharzadeh and Mehrbod Mohajer

***Abstract*—This communication describes the design, integration and measurement of a compact, wide-band, circularly polarized antenna for millimeter-wave short-range communication. The antenna is comprised of a five-section square loop and a tapered feed line. This configuration is less sensitive to the fabrication issues compared to the conventional circular spiral antennas. Two samples of this antenna designed for 60 GHz are integrated in a 6 layer IC package. The measured impedance bandwidth of the antenna-in-package is over 12 GHz. Moreover, this circularly polarized antenna provides over 7 GHz of axial ratio bandwidth. The measured peak gain is around 6 dBi. The compact-size and simple feed structure of the designed antenna make it a low-cost solution for the integrated millimeter-wave radio packaging.**

***Index Terms*—60 GHz, BGA, broadband antenna, circular polarization, flip-chipping, LGA, millimeter-wave, packaging.**

I. Introduction

Circularly polarized (CP) antennas have certain advantages over linearly polarized (LP) antennas for portable applications. For example, in a multipath environment, use of a CP antenna reduces the delay spread by about half compared to LP antennas [1]. Moreover, the performance of the CP antennas in a wireless link is less sensitive to the antenna axial

Manuscript received August 14, 2013; revised October 03, 2013; accepted October 30, 2013. Date of publication November 07, 2013; date of current version January 30, 2014.

M. Fakharzadeh is with Peraso Technologies, Antenna and Packaging, Toronto, ON M5J2L7, Canada (e-mail: mohammad@perasotech.com).

M. Mohajer is with the University of Waterloo, Electrical and Computer Engineering, Waterloo, ON N2L 3G1, Canada (e-mail: mmohajer@uwaterloo.ca).

Color versions of one or more of the figures in this communication are available online at http://ieeexplore.ieee.org.

Digital Object Identifier 10.1109/TAP.2013.2290038

rotation. However, designing a CP antenna with a low axial ratio (AR) over a relatively wide frequency band is a challenge.

Many CP antennas have a complex feed network [2]. For example, aperture coupled CP antennas usually require three layers of the packaging; the top layer for antenna, the middle layer for aperture, and the bottom layer for launcher. Use of more metal layers, which also happens for the cavity-based or multi-feed antennas, increases the packaging cost and size. Nowadays, making cellphones and laptops thinner is a milestone for consumer electronics. This highlights the importance of a low-profile radio packaging design. So, in addition to the antenna performance, size and complexity of the antenna feed are critical factors for the commercial mm-wave applications. A fully planar CP antenna with feed and antenna located on the same layer is an effective solution to reduce the packaging cost and height. This is the main target of this communication.

Various integrated CP antenna designs have been proposed for mm-wave applications [3]–[9]. These designs are either implemented in multi-layer organic packages [3], [4], LTCC technology [5]–[8], or fused silica substrate [9]. Some of these solutions are fairly expensive, thus not suitable for the high-volume consumer electronic market.

For the integrated antenna structure, different designs have been implemented at 60 GHz, such as aperture-coupled patch antenna [3], slot array [4], U-slot patch antenna array [5], multi-layer slot antenna [6], grid arrays with multiple feed points [7], helical antenna array [8], and patch antenna incorporating an air cavity and a fused silica superstrate [9].

This communication describes the design and integration of the single arm rectangular spiral antenna in a 60 GHz flip-chipped package. Single arm rectangular spiral antenna is a low profile CP antenna design, which has been designed before for lower frequencies [10], [11]. This type of antenna has a simple feed network, single layer structure, and provides a broadband, low-cost, in-package solution. The antenna has been designed to meet the requirements of 60 GHz wireless applications described in IEEE 802.11 ad, IEEE 802.15.3c, and ECMA 387 standards [12]–[14], which can be summarized as:

- minimum 9 GHz bandwidth (from 57 to 66 GHz);
- 6 dBi peak gain to transfer 2.5 Gb/s data over 5 m range (MCS 9 in IEEE 802.11ad);
- an AR less than 3 dB at the maximum gain direction over the two 60 GHz channels with worldwide coverage, i.e., from 59.4 to 63.72 GHz.

Two antennas of this type are integrated in a 6 layer organic flip-chipped package. Section II describes the antenna and antenna-in-package design. The measured performance of the fabricated antennas is presented in Section III. Section IV concludes this communication.

II. Antenna-in-Package Design

A. Single Antenna Design

Spiral antennas are known as frequency independent structures with a very broad bandwidth. Additionally, the angular dependency of spiral geometry provides the circular polarization of radiating fields. All these properties make the spiral antenna an attractive solution for broadband CP antenna. Usually, the fabrication tolerances and design rules for the trace width and spacing do not allow for better than 50 μm to 100 μm feature sizes, while conventional Archimedean spiral antennas at mm-wave require finer traces. At mm-wave frequencies, this error can change the antenna resonance or axial ratio by hundreds of MHz. To reduce the effect of fabrication errors on antenna performance, a single arm square spiral structure with five sections and four bends was designed.

Fig. 1 illustrates the designed square spiral antenna and its feed. In this type of antenna, the circumference of the loop is usually a multiple

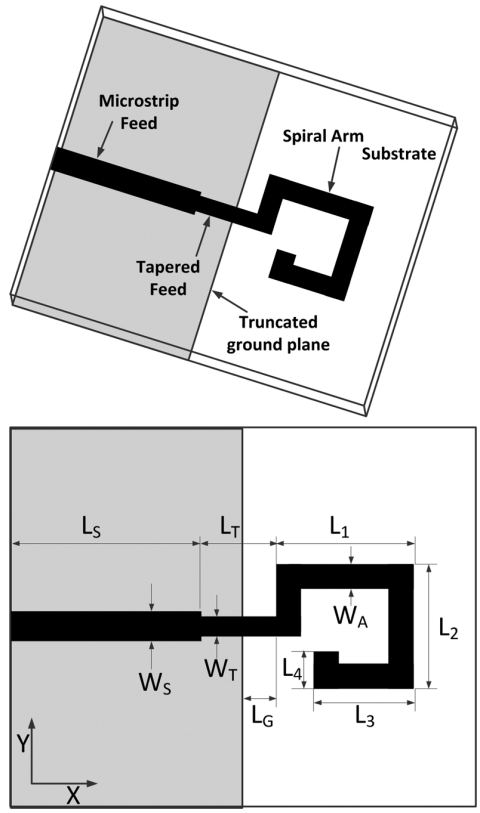

Fig. 1. Geometry of the standalone square spiral antenna.

of resonant wavelength. In this design, the arm length ($\mathrm{L}_1, \mathrm{L}_2, \mathrm{L}_3, \mathrm{L}_4$) and the spacing between the square and ground plane (L_G) are the crucial factors affecting the antenna performances. The antenna substrate selected for this design has a dielectric constant (ε_r) of 3.5, a dielectric loss ($\tan\delta$) of 0.0035 at 60 GHz, and a thickness of 5 mil ($\sim 127\ \mu\mathrm{m}$). The optimal antenna parameters, obtained from the extensive full-wave HFSS analyses, are: $L_1 = 1.9$ mm, $L_2 = 1.45$ mm, $L_3 = 1.4$ mm, $L_4 = 550\ \mu$m and $L_\mathrm{G} = 675\ \mu$m. the values of other parameters shown in Fig. 1 are as follows: $W_A = 270\ \mu$m, $W_T = 180\ \mu$m, $W_S = 280\ \mu$m, $L_5 = 2.3$ mm, and $L_T = 1$ mm. The HFSS simulation of the stand-alone antenna shows that the impedance bandwidth ranges from 50 to 70 GHz, resulting in over 33% relative bandwidth. Furthermore, the axial ratio at the maximum gain direction is less than 3 dB from 54.8 to 68.6 GHz, which confirms the circularly polarized radiation of this antenna over a wide range (23%).

As discussed in [10], the antenna peak gain direction ($\theta_{\max}$) is tilted from z-axis. It varies from 10° to 20° as the frequency changes within the 60 GHz spectrum. The standalone antenna can provide 5 dBi gain, 1 dB less than our design goal. It will be shown that the ground plane at the bottom of the package as and the modified parasitics in other layers, help to improve the antenna-in-package directivity.

B. Package Structure

The organic IC-package consists of six metal layers and five dielectric layers. The package size is 13 mm × 13 mm. The package thickness is only 0.65 mm. The top metal layer (L01) is used for both antenna etching and die flip-chipping. Fig. 2 shows the first three metal layers in the package. The top dielectric layer is the high-speed layer with a relative permittivity (ε_r) of 3.5 and dielectric loss ($\tan\delta$) of 0.0035 at 60 GHz range. Other dielectric layers are made of regular PCB material (FR4). The thickness of the copper above the high-speed layer is 18 μm. It can be reduced to 12 μm without any significant effect on the antenna performance. The second metal layer is the antenna ground

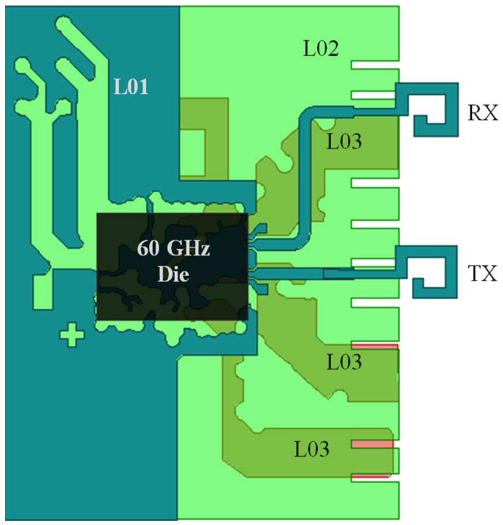

Fig. 2. Layers 1 to 3 of the package with two antennas and die.

layer. The antenna ground is truncated and can be corrugated to improve antenna radiation and matching [15], as shown in Fig. 2.

There are power planes on the 3rd and 4th metal layers of the package for sensitive power supplies. These power planes play the role of capacitors to reduce the power supply noise. There is some flexibility in designing the shape of these metal patches, which can be used to improve the antenna performance. The 5th metal layer is only used for routing, and the last layer is used for land grid array (LGA) to assemble the 60 GHz package to the main board.

C. Antenna-in-Package (AIP) Structure

The *first step* in AIP design is to add two antennas to the top layer of the package for transmit and receive. The TX and RX pads are on the same side of the 60 GHz die with 720 μm spacing. Using fine Ball Grid Array (BGA) technology, the die is flip-chipped to the antennas pads and other pads on the top layer of the package. Solder-mask defined flip-chipping method is used in this package. The solder bump pad size is 100 μm, and the opening in solder mask is 80 μm. The solder bump is around 80 μm. The die-pad pitch is 180 μm, while the 50 ohm line width is 275 μm. Thus, each antenna feed is tapered and connected to the corresponding RF pad trough a compact, low loss microstrip to CPW line transition.

The two antennas should be separated to enhance the isolation between the TX and RX paths. Hence, as shown in Fig. 2, the RX antenna feed line is bent to sufficiently separate the RX and TX antenna positions. For sake of practical measurements, the TX antenna has a shorter and a straight feed line. Note that the antenna positions with respect to the other metal layers can affect the antenna performance. Thus, the *second step* in AIP design is to apply full EM analysis to the package to investigate how the antenna performance is affected by the packaging elements. EM analyses show that the antenna performance is mainly affected by the parasitic elements on layer 3 and the ground on layer 6. Layer 6 is used for LGA assembly, so there is no flexibility in modifying this layer. Nevertheless, the authors have found three experimental methods to modify the parasitic elements on layer 3 and 4:

1. designing the parasitic elements as resonant structures at the frequency of operation; or
2. designing them as reflectors; or
3. reducing their effects by meshing and/or truncation.

The 1st and 2nd methods are more appropriate for linearly polarized antennas. For example, method 2 results in 1–2 dB gain improvement for a planar Yagi antenna. For a CP antenna, these two methods increase maximum gain of the antenna but degrade the AR bandwidth. After taking these considerations into account, layer 3 was modified in the shape illustrated in Fig. 2. These parasitic elements are power plains designed to decrease the power supply noise.

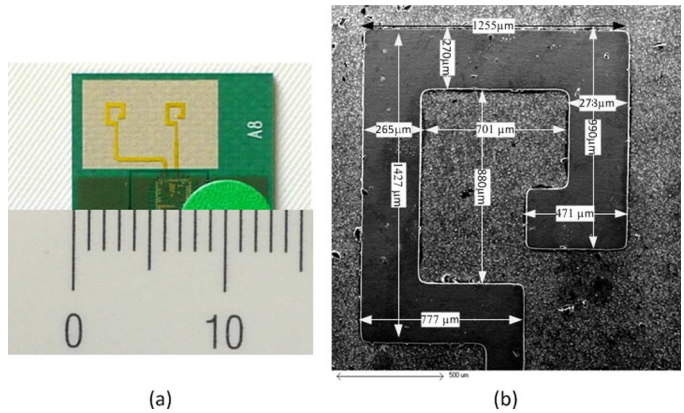

Fig. 3. (a) Top view of the fabricated single arm rectangular spiral antennas-in-package. (b) SEM image of the fabricated antenna with the measured dimensions.

The *third step* in AIP design is to modify the antenna dimensions to compensate for the layer 6 (lower ground layer) effects as well as other layers in the package. Compared to the antenna designed in Section II.A, the following modifications in Square Spiral dimensions were made. Referring to parameters shown in Fig. 1, L_1, $L_2 L_3$, and L_4 were reduced to 1550 μm, 1380 μm, 1150 μm, and 470 μm, respectively. The width of transmission line which forms the arm (W_A) increased to 300 μm. The length of the TX antenna feed-line is 3.5 mm, and the optimal center-to-center distance between the two antennas is obtained as 3.9 mm. For this antenna spacing, simulations show that the isolation between the two antennas is better than 19 dB over the 60 GHz spectrum.

The ground plane size on layer 2 was optimized for the best impedance matching. It is possible to use corrugated ground plane to improve the impedance matching, but it has an adverse effect on the axial ratio of the antenna. To achieve the required AR, the corrugation slots were removed in the finalized AIP design. Finally, the antenna-in-package is electromagnetically simulated to find the AIP performance. Results will be presented in Section III.

D. Post-Fabrication Analysis

One way to evaluate the packaging fabrication errors is to take high resolution images of the fabricated package, and measure the antenna features. Fig. 3(a) shows the fabricated package with both antennas. Fig. 3(b) shows a high resolution scanning electron microscope (SEM) image of the fabricated sample with the measured dimensions. Compared to the design values, shrinkage of 4.5% to 8% is observed in the fabricated sample. Shrinkage is an offset error, which can be compensated in the next round of fabrication, if the same packaging technology is to be used. The dimensions shown in the SEM image were used for post-fab simulations, in the next section, to analyze the measured results realistically.

III. Simulated and Measured AIP Results

A. Bandwidth

Fig. 4 shows the simulated and measured reflection coefficients (S_{11}) of the TX antenna. For this measurement, fabricated package samples were measured without die (no flip-chipping) using a probe-station. The CPW side of the antenna feed was excited by network analyzer (N5247A PNA-X) via 175 μm GSG probe. The setup was calibrated

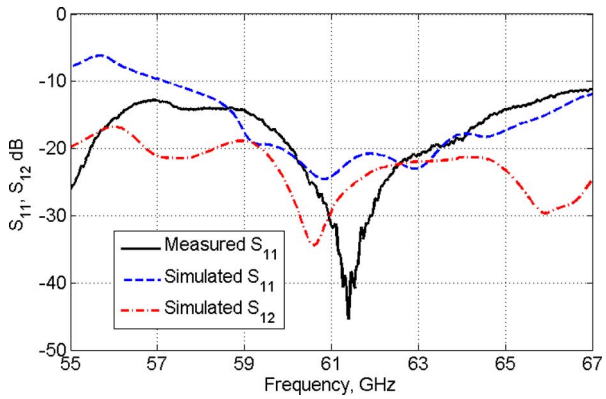

Fig. 4. Measured and simulated reflection coefficient of the TX antenna-in-package, and the coupling between RX and TX antennas.

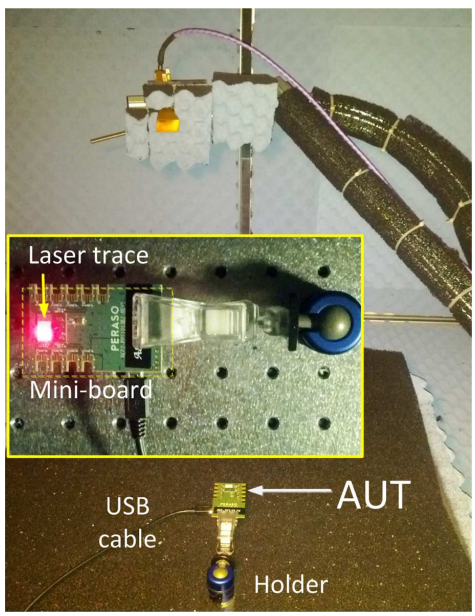

Fig. 5. Antenna pattern measurement in an advanced anechoic chamber. The inset shows the package assembled to a test-board. The laser trace is used to position AUT at the center of the chamber.

up to the tip of the probe with short-open-load-thru (SOLT) calibration technique. The measured results show the 10-dB antenna bandwidth extends to the beyond of the measured frequency range from 55 GHz to 67 GHz. The measured antenna matching is slightly better than the simulated matching, probably because some parts of the packaging layers were simplified in simulations. Fig. 4 depicts that the simulated isolation between the two antennas ($-S_{12}$) is better than 19 dB over the 12 GHz frequency range.

B. Radiation Pattern and Gain

The setup used to measure the maximum gain and radiation pattern of the antenna is shown in Fig. 5. The 60 GHz package was assembled to a mini-board, which provides the bias and external filtering for the circuitry. The board placed inside the anechoic chamber, is programmed through a micro-USB port. A reference horn antenna is located at the far-field region, which scans the surface of a quarter-sphere using two motors and arms with steps of 1 degree. A laser beam is used to help positioning the antenna. The TX antenna is excited by the die. Using the PLL of the 60 GHz die, the transmitter carrier can change from 58.32 to 64.8 GHz with steps of 2.16 GHz. The received power by the standard horn antenna was measured by the power meter. The measured power was used to extract the antenna gain and pattern at each angular position.

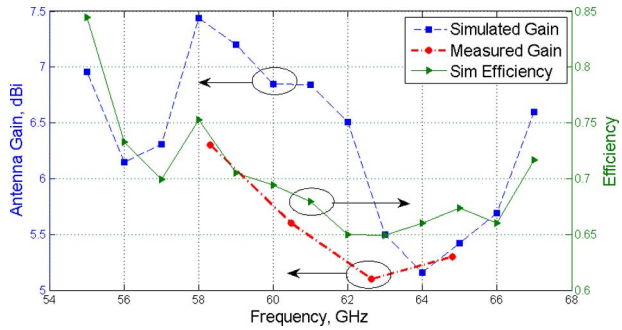

Fig. 6. The simulated and measured maximum antenna gain and simulated radiation efficiency over the 60 GHz frequency range.

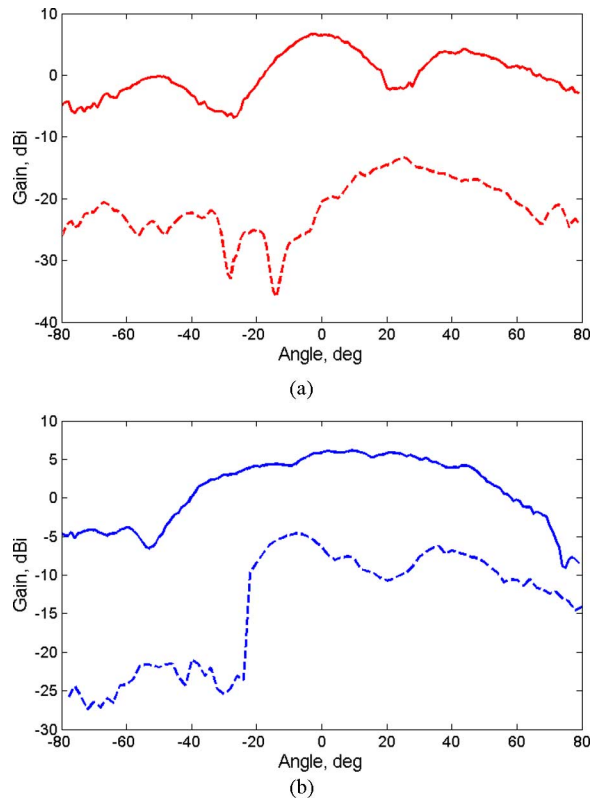

Fig. 7. Measured LH (solid) and RH (dashed) patterns of the antenna at 60 GHz in (a) $\varphi = 0°$, and (b) $\varphi = 90°$.

Fig. 6 shows the simulated and measured maximum gain, and the radiation efficiency of the TX antenna. As the frequency increases from 58 to 64 GHz the simulated maximum gain drops from 7.4 dBi to 5.1 dBi. The measured maximum gain is in good agreement with the simulations and confirms this trend. However, it is slightly lower than the simulated values, changing from 6.3 dBi to 5 dBi over the desired frequency band. The error in maximum gain measurement is around 1 dB. The main sources of error are power meter error and arm positioning error (1°). Moreover, the reflections from the mini-board affect the antenna radiation pattern. Fig. 6 shows that the antenna efficiency, including the feed line, and CPW transition to die, ranges from 65% to 76% in the 60 GHz spectrum.

Fig. 7 shows the measured left hand (LH) and right hand (RH) radiation patterns at 60 GHz in $\varphi = 0°$ (XZ) and (b) $\varphi = 90°$ (YZ) planes defined according to Fig. 1. In $\varphi = 90°$ plane, the beam is broader and the peak is tilted by 10°.

C. Axial Ratio

Fig. 8 compares the measured and simulated axial ratios of the TX square spiral antenna versus frequency at the maximum gain direction.

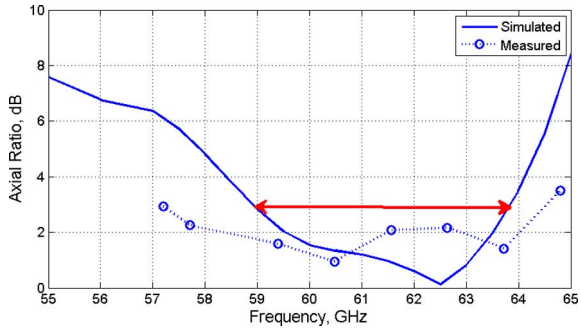

Fig. 8. Simulated and measured antenna-in-package AR over the 60 GHz frequency range.

Simulated results show that the antenna has an AR bandwidth of 5 GHz. Measurements show that the AR bandwidth is close to 7 GHz.

IV. Conclusions

It was shown that the single arm rectangular spiral antenna is a suitable solution for mm-wave short range application. This antenna provides circular polarization with a compact and simple structure. This antenna has a broadband performance with 33% relative bandwidth. The axial ratio bandwidth of this antenna can be as large as 22%. The designed antenna can be easily integrated in a multi-layer package. The antenna structure can be modified to compensate for the packaging effects. The measured results for a 60 GHz implementation of the square spiral antenna in-package show more than 12 GHz of impedance bandwidth, 7 GHz of axial-ratio bandwidth, and 6 dBi gain. The antenna efficiency, calculated at the die pad, ranges from 65% to 75%. Use of this fully planar CP antenna, where feed and antenna located on the same layer, reduces the packaging cost and height significantly.

References

[1] T. Manabe, Y. Miura, and T. Ihara, "Effects of antenna directivity and polarization on indoor multipath propagation characteristics at 60 GHz," *IEEE J. Sel. Areas Commun.*, vol. 14, no. 3, pp. 441–448, 1996.

[2] K.-L. Wong, *Compact and Broadband Microstrip Antennas*, 1st ed. New York, NY, USA: Wiley-Interscience, 2002.

[3] D. Liu, J. A. Akkermans, H.-C. Chen, and B. Floyd, "Packages with integrated 60-GHz aperture-coupled patch antennas," *IEEE Trans. Antennas Propag.*, vol. 59, no. 10, pp. 3607–3616, Oct. 2011.

[4] A. R. Weily and Y. J. Guo, "Circularly polarized ellipse-loaded circular slot array for millimeter-wave WPAN applications," *IEEE Trans. Antennas Propag.*, vol. 7, no. 10, pp. 2862–2870, Oct. 2009.

[5] H. Sun, Y.-X. Guo, and Z. Wang, "60-GHz circularly polarized U-slot patch antenna array on LTCC," *IEEE Trans. Antennas Propag.*, vol. 61, no. 1, pp. 430–435, Jan. 2013.

[6] Y. P. Zhang, M. Sun, K. M. Chua, L. L. Wai, and D. Liu, "Antenna-in-package design for wirebond interconnection to highly integrated 60-GHz radios," *IEEE Trans. Antennas Propag.*, vol. 57, no. 10, pp. 2842–2852, Oct. 2009.

[7] B. Zhang and Y. P. Zhang, "Grid array antennas with subarrays and multiple feeds for 60-GHz radios," *IEEE Trans. Antennas Propag.*, vol. 60, no. 5, pp. 2270–2275, May 2012.

[8] C. Liu, Y.-X. Guo, X. Bao, and S.-Q. Xiao, "60-GHz LTCC integrated circularly polarized helical antenna array," *IEEE Trans. Antennas Propag.*, vol. 60, no. 3, pp. 1329–1335, Mar. 2012.

[9] R. Zhou, D. Liu, and H. Xin, "Design of circularly polarized antenna for 60 GHz wireless communications," in *Proc. EuCAP*, 2009, pp. 3787–3789.

[10] H. Nakano, J. Eto, Y. Okabe, and J. Yamauchi, "Tilted- and axial-beam formation by a single-arm rectangular spiral antenna with compact dielectric substrate and conducting plane," *IEEE Trans. Antennas Propag.*, vol. 50, no. 1, pp. 17–23, Jan. 2002.

[11] J. T. Bernhard, "Compact single-arm square spiral microstrip antenna with tuning arms," in *Proc. IEEE Int. Antennas Propagation Symp.*, Jul. 8–13, 2001, vol. 2, pp. 696–699.

[12] M. Fakharzadeh *et al.*, "CMOS phased array transceiver technology for 60 GHz wireless applications," *IEEE Trans. Antennas Propag.*, vol. 58, no. 4, pp. 1093–1104, Apr. 2010.

[13] M. Fakharzadeh and L. Verma, "PHY front end design for emerging 60 GHz multi-gigabit wireless devices," in *Proc. 10th IEEE CCNC*, Las Vegas, NV, USA, Jan. 2013, pp. 817–820.

[14] L. Verma, M. Fakharzadeh, and S. Choi, "Wi-Fi on steroids: 802.11ac and 802.11ad," *IEEE Wireless Commun. Mag.*, vol. 20, no. 6, pp. 30–35, Dec. 2013.

[15] R. A. Alhalabi, Y. C. Chiou, and G. M. Rebeiz, "Self-shielded high-efficiency Yagi-Uda antennas for 60 GHz communications," *IEEE Trans. Antennas Propag.*, vol. 59, no. 3, pp. 742–750, Mar. 2011.

Compact Antenna With U-Shaped Open-End Slot Structure for Multi-Band Handset Applications

Cho-Kang Hsu and Shyh-Jong Chung

***Abstract*—This communication proposes a compact U-shaped slot antenna with a coupling feed for 4G handset applications. The antenna is composed of a simple open-end U-shaped slot and a feeding line with an antenna area of 58 mm × 12 mm. Two types of resonant modes are excited, including slot mode and monopole mode. Parametric studies on the slot geometry have been demonstrated. By controlling the related parameters, the bandwidth of this antenna can potentially cover the mobile bands of LTE Band 12 (698–742 MHz)/DCS (1710–1880 MHz)/PCS (1850–1990 MHz)/UMTS (1920–2170 MHz)/LTE Band 40 (2300–2400 MHz)/Band 41 (2496–2690 MHz)/Band 42 (3400–3600 MHz)/Band 43 (3600–3800 MHz). Good radiation characteristics, like gain and radiation efficiency are obtained over these operating bands. This antenna is suitable for the metal casing of handheld devices.**

***Index Terms*—Cellular phone antennas, mobile phone antennas, multi-band antenna, slot antenna.**

I. Introduction

With the growing demand for communication systems, antennas on handheld devices are needed to support multiple bands of 2G, 3G and 4G. Handheld devices are preferred to be light-weight, thin, and fashionable, and as a result, metal casings have become popular. However, the bandwidth and radiation efficiency of conventional antennas in handheld devices tend to decrease when antenna in proximity of metal casings. Examples include the monopole and inverted-F antennas. Therefore, slot antennas become attractive for handheld devices with metal casings.

Various slot antenna structures, including circular [1], triangles [2] and fractal shape [3], have been proposed to achieve a wide impedance bandwidth. A wide slot might support numerous resonance modes, and two nearby resonance modes can be merged to form a wider bandwidth [4]. However, because these designs require a large area for slot, they are not suitable for handheld devices.

To reduce the overall size of a multi-band slot antenna, various designs have been produced. Some quarter-wavelength open slots are designed in [5] and [6] to achieve a compact size. In [7] and [8], multiple bandwidths are achieved with several independent slots that operate

Manuscript received May 28, 2013; revised August 19, 2013; accepted October 24, 2013. Date of publication November 07, 2013; date of current version January 30, 2014.

The authors are with the Department of Communication Engineering, National Chiao-Tung University, Hsinchu 300, Taiwan, ROC (e-mail: drokun.tw@gmail.com; sjchung@cm.nctu.edu.tw).

Digital Object Identifier 10.1109/TAP.2013.2289996